Ultrahigh-Resolution ^{7}Li MAS NMR Spectroscopy by Isotopic Dilution

Vladimir K. Michaelis,[a,†,*] Kirill Levin,[a] Yaroslav Germanov,[a] Gérald Lelong[b] and Scott Kroeker[a,*]

[1]*Department of Chemistry, University of Manitoba, Winnipeg, Manitoba, Canada, R3T 2N2*

[2]*Institut de Minéralogie de Physique des Matériaux et de Cosmochimie (IMPMC), Sorbonne Universités – UPMC, Jussieu, 75005, Paris, France*

ABSTRACT: The functional importance of lithium in many types of materials requires reliable methods to study its local structure and dynamics. Nuclear magnetic resonance (NMR) spectroscopy should be ideal for this purpose, but suffers from poor resolution due to intrinsic dipolar broadening. We overcome this problem by diluting the ^{7}Li spins with ^{6}Li, producing ultrahigh-resolution ^{7}Li magic-angle spinning (MAS) NMR spectra of lithium borates without appreciably sacrificing sensitivity. Resolution of up to six distinct lithium environments permits assignments, aided by density-functional theory, which indicate separate chemical shift regions for different coordination numbers. With high sensitivity and site-specific Li resolution, two-dimensional NMR methods for probing Li hopping become more informative, revealing preferential site exchange in a complex lithium borate phase. The success of this approach will make ^{7}Li MAS NMR an attractive method for probing lithium coordination environments and mobility in diamagnetic lithium-bearing materials.

Lithium is a functional component in a vast array of materials, including battery cathodes,[1-5] ion-conducting organic polymers,[6] non-linear optical crystals,[7] pharmaceuticals such as anti-depressants,[8] dental cements[9, 10] and glass-ceramics,[11, 12] impacting diverse areas of research ranging from health and medical sciences to earth and environmental sciences.[13, 14] Essential to the development of next-generation lithium-bearing materials are research tools to accurately and efficiently characterize lithium local structure and dynamics in solids, so as to better understand its specific functional role. However, its small x-ray scattering cross-section and its propensity to diffuse amongst adjacent sites makes it difficult to locate by laboratory-based diffraction methods as well as atom-specific probes such as x-ray absorption spectroscopy. As a result, solid-state nuclear magnetic resonance (NMR) spectroscopy has emerged as an indispensable tool for the characterization of lithium chemical environments in materials.[13, 15-18]

The attractiveness of ^{7}Li as a probe nucleus in NMR derives from its high receptivity (^{1}H=1.0; ^{7}Li = 0.271; ^{13}C = 0.0001), stemming from its high natural abundance (92.5%) and large magnetogyric ratio (γ = 10.397 x 10^{7} rad s^{-1} T^{-1}). Although ^{7}Li is quadrupolar (I = 3/2), its quadrupole moment is very small and has a negligible influence on the central transition at typical NMR magnetic fields, such that it can generally be treated as a spin-1/2 nuclide. Because of these advantages, ^{7}Li magic-angle spinning (MAS) NMR has played a prominent role in the advancement of lithium batteries, where the paramagnetic nature of most cathode materials produces large contact shifts up to ~1000 ppm and in some cases up to 2500 ppm, resulting in dramatic gains in spectral resolution.[1, 19, 20] For example, ^{7}Li NMR has provided key insights into the structure and function of lithium cobalt oxide ($LiCoO_2$) cathodes, which possess high energy density and are valuable components of commercial lithium-ion batteries.[5, 21, 22] Unfortunately, ^{7}Li NMR is less effective for diamagnetic solids, where the total chemical shift range is less than 5 ppm in oxides,[23] for example, precluding the resolution of site-specific information about local chemical environments and hopping between them. Besides its narrow chemical shift range, ^{7}Li NMR resolution is hampered by peak broadening due principally to strong homonuclear dipolar coupling between nearby ^{7}Li spins with a large magnetogyric ratio and high natural abundance. The inability of MAS to completely attenuate this broadening typically leads to peak widths which span the entire chemical shift range of diamagnetic compounds, limiting its chemical applications.

This broadening is analogous to that which prevents widespread use of ^{1}H NMR in the structural elucidation of organic solids. The well-known effectiveness of MAS for eliminating heteronuclear dipolar couplings does not extend simply to homonuclear couplings, which becomes a critical obstacle to spectral resolution in materials with high-sensitivity nuclei present in abundance. For example, strong ^{1}H-^{1}H dipolar coupling inhibits high-resolution ^{1}H MAS NMR spectroscopy of complex proteins and peptides, and many of the innovations in this area have come from the biomolecular community. Historically, appreciable linewidth reductions have been realized using a combination of moderate spinning frequencies and homonuclear decoupling pulse sequences such as WAHUHA[24], CRAMPS[25] or Lee-Goldburg[26] decoupling. More recently, advances in MAS probe technology have increased maximum spinning frequencies to above 100 kHz,[27] improving resolution through better, but still incomplete averaging of strong homonuclear dipolar couplings.[28-30] Aside from the high cost of such probe systems, distinct disadvantages include severely restricted sample volumes (i.e., nanoliters) and considerable frictional heating effects, requiring active cooling to avoid sample dehydration and/or degradation. An alternative method to reducing homonuclear dipolar couplings was presented in the early 1990s, where dilution of proton spins by reverse isotopic labeling with deuterium

significantly improved resolution in perdeuterated biomolecular solids,[31-35] even at modest spinning frequencies.[36, 37] Combining faster spinning (> 40 kHz) with perdeuteration has led to advances using direct ^{1}H NMR detection of proteins.[38] This approach offers very high resolution (< 0.2 ppm) linewidths and enhanced sensitivity in biomolecular solids through ^{1}H detection and *J*-based transfers.[38-40]

In this work, we demonstrate ultrahigh-resolution ^{7}Li MAS NMR spectroscopy of crystalline and amorphous lithium-bearing materials using isotopic dilution by ^{6}Li to interrupt the strongly coupled network of ^{7}Li spins, and MAS to eliminate broadening from the resulting ^{6}Li-^{7}Li heteronuclear dipolar interactions. The substantial peak width reductions obtained by this method are sufficient to resolve multiple lithium sites in a series of lithium borates, which display rich structural diversity and are under scrutiny as solid electrolytes for next-generation lithium batteries.[41, 42] The high sensitivity of ^{7}Li is retained even at moderate spinning rates and external magnetic fields, facilitating quantitative NMR analysis in practical time frames and enabling 2D NMR methods for monitoring Li ion dynamics.

Several crystalline lithium borates were studied by ^{7}Li MAS NMR in their natural abundance and ^{7}Li-depleted (5%) forms to evaluate the benefits of isotopic dilution on spectral resolution and sensitivity. Lithium metaborate, $LiBO_2$, containing a single crystallographic Li site, yields an eight-fold reduction in the ^{7}Li MAS NMR peak width upon ^{7}Li depletion, the full-width at half maximum (FWHM) decreasing from 1080 to 140 Hz at a modest spinning rate of 16 kHz (data not shown). There are six lithium ions within a 4 Å radius, the closest being 2.6 Å, corresponding to a 1 kHz dipolar coupling constant. The significance of ^{7}Li-^{7}Li dipolar broadening in the natural abundance sample is underscored by increasing the spinning rate to 60 kHz, which reduces its MAS peak width by a factor of three (340 Hz, Figure 1) relative to the 16 kHz spectrum. Combining isotopic dilution with fast spinning results in an overall 15-fold improvement in resolution for $LiBO_2$ (FWHM ~70 Hz, 0.3 ppm).

At natural abundance, the three crystallographically inequivalent sites of lithium orthoborate, Li_3BO_3, appear in fast-spinning ^{7}Li MAS NMR (ν_r = 60 kHz) as a single undifferentiated broad peak (Figure 1). In this case, the lithium spin network is more highly coupled, with 13 lithium neighbors within a 4 Å radius. Depleting the ^{7}Li in the sample to 5% simplifies the spin system, revealing two distinct ^{7}Li peaks in a ~2:1 intensity ratio, with similar resolution at moderate and fast spinning rates (ν_r = 16 or 65 kHz, Figures 1 and S1). Considering that the structure possesses two five-coordinate Li sites and one four-coordinate Li, this spectrum may be assigned according to established correlations between coordination number and chemical shift (vide infra).[43, 44] The four-coordinate peak width is less than 40 Hz (0.2 ppm), a 20-fold improvement in resolution. Comparable resolution may be obtained from ^{6}Li MAS NMR of a natural abundance sample (7.5% ^{6}Li), however at a staggering cost in experimental time. Whereas 3 mg of ^{7}Li-depleted Li_3BO_3 required only 30 minutes to acquire the spectrum shown in Figure 1, a natural-abundance ^{6}Li MAS NMR spectrum with similar signal-to-noise required over 140 minutes with an order-of-magnitude more sample (30 mg) to achieve comparable signal-to-noise. The ^{6}Li-enriched starting materials used to dilute the ^{7}Li spins are inexpensive compared to other common isotopes used in NMR; for example, ^{6}Li-enriched Li_2CO_3, LiCl and Li (~$0.2/mg, 95% ^{6}Li) compare to ^{13}C-labeled amino acids and sugars (~$0.4/mg glucose, 99% ^{13}C), ^{17}O-labeled water (~$4.5/mg, 90% ^{17}O) and $^{119}SnCl_2$ (~$15.0/mg, 97% ^{119}Sn). The high spectral resolution, combined with small sample requirements and high ^{7}Li sensitivity, make this an attractive and cost-effective method for other Li-bearing materials.

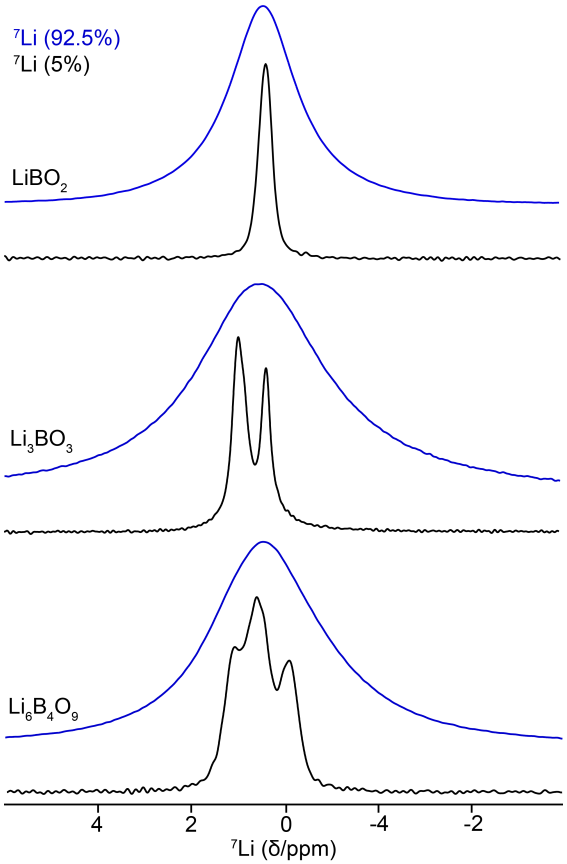

Figure 1. ^{7}Li MAS NMR (B_0 = 11.7 T, ν_r = 60 kHz) of depleted (5% ^{7}Li, black traces) and naturally abundant (92.5% ^{7}Li, blue traces) $LiBO_2$, Li_3BO_3 and $Li_6B_4O_9$.

A more stringent test of this method is $Li_6B_4O_9$, which possesses six distinct crystallographic lithium sites.[45] Fast-spinning ^{7}Li MAS NMR of the natural abundance sample yields a familiar broad and featureless peak with only a hint of asymmetry (Figures 1 and S2), whereas the ^{7}Li-depleted sample reveals multiple partially resolved peaks. In conjunction with quantum-chemical calculations, these peaks can be reasonably assigned to the six Li sites in the compound (Table S1, vide infra). The ^{6}Li MAS NMR spectrum of the isotopically diluted sample is provided for comparison (Figure S2), exhibiting poorer resolution than ^{7}Li MAS NMR of this sample and at the expense of ~50-fold increase in experimental time (15 hours *vs* 20 min). This extreme difference in practical sensitivity is due principally to the much longer nuclear spin-lattice relaxation time (T_1); whereas the ^{7}Li T_1 values in these samples are not short, ranging from 2 to 15 minutes, attempts to measure the ^{6}Li T_1s were unsuccessful, as full relaxation had not been achieved after more than 4 hours. Interestingly, ^{7}Li T_1 values are very similar in the natural abundance and ^{7}Li-depleted samples, suggesting that relaxation is dominated by quadrupolar effects and not significantly influenced by homo-

nuclear dipolar interactions. In all of these samples, the ^{6}Li NMR spectral resolution of natural abundance samples is comparable but slightly worse than that of ^{7}Li in the depleted samples, leading to inferior detection of multiple lithium sites. Since the chemical shift ranges of different isotopes of the same element are identical when measured in parts-per-million, resolution will be largely based on their respective magnetogyric ratios. For Li, the very small chemical shift range in oxides (~4 ppm) requires a large external magnetic field to quench the second-order quadrupolar broadening and achieve adequate peak resolution, even if homonuclear dipolar interactions are minimized by isotopic depletion. For example, matching the Hz/ppm resolution of ^{7}Li at a typical laboratory field of 14.1 T (600 MHz, ^{1}H) would require an external magnetic field of more than 35 T (> 1500 MHz, ^{1}H) for ^{6}Li. The combination of lower site resolution and significantly longer experimental times for ^{6}Li NMR spectroscopy makes severe demands on the instrumentation and limits options for more advanced multidimensional approaches. Considering the prohibitive purchase and operational costs of ultrahigh-field magnets and that the state-of-the-art commercial target is "only" 1.5 GHz, ^{7}Li depletion is an inexpensive and effective experimental approach to overcome ^{7}Li-^{7}Li broadening interactions in lithium-containing materials.

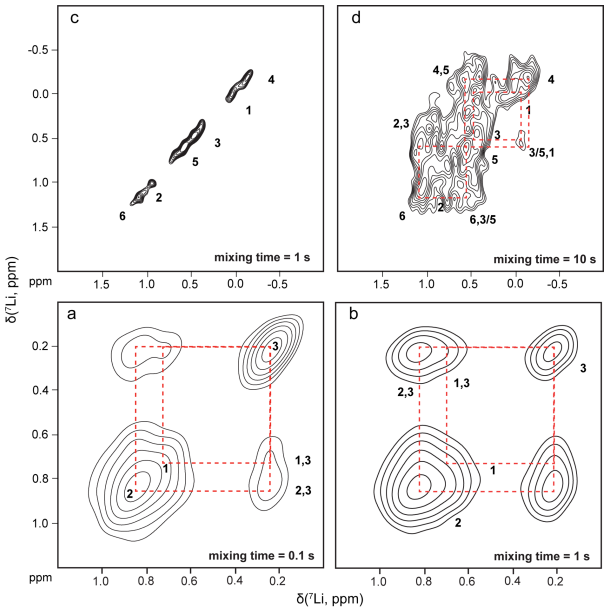

Figure 2. Two-dimensional ^{7}Li EXSY MAS NMR (B_o = 11.7 T, ν_r = 60 kHz) contour plots of (a,b) Li_3BO_3 and (c,d) $Li_6B_4O_9$, with the specified mixing times. Peak assignments are from quantum chemical calculations (see text).

Lithium NMR is commonly used to study chemical environments and dynamics in solid-state materials. For example, much has been learned by $^{6/7}$Li MAS NMR about the structure and function of materials for lithium batteries such as $Li[Ni_{1/3}Mn_{1/3}Co_{1/3}]O_2$,[46] Cr-doped $LiCoO_2$ (or $LiMnO_2$),[47] and $LiVPO_4F$.[48] Resolution in these systems originates principally from the contact interaction due to unpaired electron density at the nucleus. In diamagnetic systems like solid-state electrolytes, site-specific ^{7}Li resolution is rarely observed and ionic mobility must often be inferred from NMR line widths, T_1 values or subtle changes in the breadth of unresolved 2D contours in exchange spectroscopy.[49] The enhanced resolution made possible by ^{7}Li depletion opens the door to site-specific information about lithium dynamics in diamagnetic solids using two-dimensional exchange spectroscopy (EXSY). Figure 2 shows the ^{7}Li EXSY 2D contour plots of Li_3BO_3 and $Li_6B_4O_9$ with mixing times ranging from 0.1 to 10 seconds. Lithium orthoborate clearly shows exchange between the resolved sites at a mixing time as short as 100 ms (Figure 2a), with the cross-peak intensity growing with mixing time (Figure 2b). The short mixing-time plot shows evidence of the two Li sites which are unresolved in the 1D data set, despite being separated by less than 0.2 ppm. The much more complex $Li_6B_4O_9$ also exhibits lithium exchange in EXSY NMR, albeit on a longer timescale. Whereas no exchange is observed with a mixing time of 1 s (Figure 2c), a 10 s mixing time reveals significant lithium migration amongst four of the six lithium sites (Figure 2d); only after 40 seconds is hopping amongst all six sites observed (Figure S3). These experiments reveal qualitatively that exchange occurs most readily amongst the four-coordinate sites (2, 5, 6, labeled according to the published crystal structure[45]), whereas intersite diffusion is slower for the five-coordinated sites (1, 3, 4). While a comprehensive analysis of the ionic hopping is beyond the scope of this work, it is worth noting that ^{7}Li isotopic dilution reduces the likelihood of interference from spin diffusion, simplifying the spectral interpretation in terms of cation mobility, even at long mixing times. Finally, we point out that the EXSY data shown in Figure 2 were all acquired with 3 mg of ^{7}Li-depleted sample and eight co-added transients per slice, implying that isotopic dilution should not hamper other multidimensional correlation NMR experiments.

The unprecedented gain in ^{7}Li NMR resolution shown here provides an opportunity to evaluate the influence of lithium coordination on the isotropic chemical shift. Figure 3a shows the excellent agreement (R^2 = 0.94) between experimental ^{7}Li isotropic chemical shift data and those predicted using quantum-chemical gauge including projected augmented wave (GIPAW) calculations, inspiring confidence in using this approach to assign the observed peaks to specific Li crystallographic sites. For the borates studied here, four-coordinate lithiums, $^{[4]}$Li, are found above +0.7 ppm, whereas $^{[5]}$Li appear between -0.2 and +0.8 ppm. This follows the trend documented for many other cations, such as ^{29}Si, ^{27}Al, ^{11}B, ^{73}Ge, ^{25}Mg, ^{133}Cs, whereby a decrease in coordination number - or a reduction in average bond length (Figure 3b) - is associated with a shift to higher frequency.[14, 50-58] Further partitioning of the $^{[5]}$Li region to reflect specific geometric arrangements of the oxygen ligands is tempting, with trigonal-bipyramidal-like geometries appearing in the lower part of the $^{[5]}$Li chemical shift range and square-pyramidal-like geometries at higher chemical shifts. Using the τ parameter previously defined to reflect a structural transition from idealized trigonal-bipyramidal (τ_5 = 1) to square-pyramidal (τ_5 = 0) geometry[59] yields a suggestive trend (Figure S4), but the small data set (n = 6) renders any conclusions speculative. While none of the compounds investigated here contains six-coordinate lithium, Xu and Stebbins reported ^{6}Li chemical shifts for $^{[6]}$Li in lithium silicates from -0.5 to -1.5 ppm, extending the correlation.[14] It is worth pointing out that ^{7}Li MAS NMR peaks in diamagnetic oxides with naturally abundant ^{7}Li are often as wide as the entire Li chemical shift range, and only with the ultrahigh resolution afforded by ^{7}Li depletion can these well-known correlations between chemical shift and coordination environment be exploited to gain structure information. Considering the weak x-ray scattering cross section of lithium and its propensity to diffusion,

taking advantage of the high resolution of ^{7}Li MAS NMR in this way may prove to be one of the most effective methods for identifying lithium local structure and dynamics in many Li-based materials.

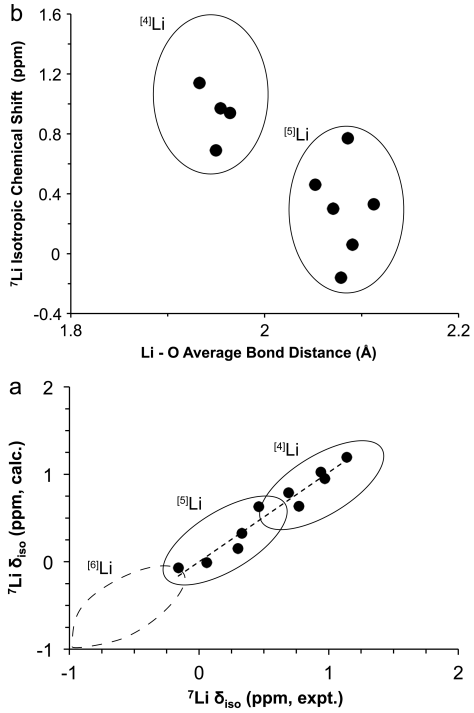

Figure 3. (a) GIPAW calculated isotropic chemical shifts ($\delta_{iso, calc}$) as a function of experimentally determined isotropic chemical shift ($\delta_{iso, expt}$) for three lithium borate crystals (R^2=0.94). (b) ^{7}Li isotropic chemical shifts as a function of average Li-O bond distances for the lithium borates studied here. Ovals denote Li coordination number ranges from four- to six-fold coordinate, where [6]Li data are from reference 14.

To further assess the capabilities of this method, ^{7}Li-depleted lithium borate glasses were prepared in an attempt to resolve distinct Li sites in structurally disordered solids. Significant line width reductions were observed upon isotopic depletion, with the resulting widths all in the 200-300 Hz range: glasses with high lithium content exhibited a five-fold reduction in width, whereas lithium-poor glasses narrowed by less than a factor of two (Table S3, Figure S5). Despite the clear attenuation of homonuclear dipolar coupling, no evidence of multiple Li chemical environments was observed. This may be jointly attributed to the distribution of lithium environments intrinsic to amorphous solids, and the ionic mobility in these glasses, variants of which are under consideration as solid-state electrolytes.[13, 15, 60-63]

Other potential applications of ^{7}Li-depletion MAS NMR take advantage of the high spectral resolution that can be obtained even at slow spinning rates. For example, the measurement of hindered lithium diffusion at low temperatures would require MAS NMR experiments at cryogenic temperatures, where spinning rates are limited.[64, 65] Likewise, the low-temperature demands of dynamic nuclear polarization NMR restrict spinning rates to ≤ 40 kHz.[66-68] Similarly, high-temperature MAS NMR probes can only reach spinning speeds of around 4 kHz, necessitating isotopic dilution to achieve site resolution in lithium compounds in situ. Finally, the determination of ^{7}Li quadrupole couplings in solids typically requires the observation of a manifold of satellite-transition spinning sidebands at lower spinning rates, which is at cross-purposes with maximal resolution in natural-abundance samples. By ^{7}Li depletion, site-specific ^{7}Li NMR resolution may be retained in spinning sidebands even at slow spinning speeds, facilitating estimates of quadrupolar parameters for multiple sites.

We demonstrate ultrahigh-resolution one- and two-dimensional ^{7}Li MAS NMR spectra of diamagnetic solids by ^{7}Li isotopic depletion. Despite a substantial reduction in the number of ^{7}Li spins, this approach retains the benefits of ^{7}Li NMR, including high sensitivity and fast spin-lattice relaxation rates relative to those of ^{6}Li, while reducing ^{7}Li homonuclear dipolar coupling to provide unprecedented resolution in diamagnetic solids under moderate MAS. In conjunction with improved MAS technology (> 60 kHz) and 2D exchange spectroscopy, three crystallographically inequivalent lithium sites were resolved within a 1 ppm chemical shift range, and up to six lithium sites assigned using quantum-chemical calculations, leading to valuable structural correlations. This simple method holds great promise for structural and dynamic studies of diamagnetic lithium-bearing materials, with potential applications in NMR crystallography and dynamic nuclear polarization.

ASSOCIATED CONTENT

Supporting Information

The Supporting Information is available free of charge on the ACS Publications website. Experimental, ^{7}Li NMR and DFT results.

AUTHOR INFORMATION

Corresponding Authors

V. Michaelis – vladimir.michaelis@ualberta.ca
S. Kroeker – Scott.Kroeker@umanitoba.ca

Present Addresses

†*Department of Chemistry, University of Alberta, Edmonton, Alberta, Canada, T6G 2G2*

ACKNOWLEDGMENT

The authors are grateful to the Natural Sciences and Engineering Research Council of Canada (NSERC) Discovery Grant Program for supporting this research. We thank Dr. V. Terskikh for performing GIPAW calculations at the Canadian National Ultrahigh-Field NMR Facility for Solids (http://nmr900.ca).

REFERENCES

1. Lee, Y. J.; Wang, F.; Grey, C. P., ^{6}Li and ^{7}Li MAS NMR Studies of Lithium Manganate Cathode Materials. *J. Am. Chem. Soc.* **1998,** *120* (48), 12601-12613.
2. Cahill, L. S.; Chapman, R. P.; Kirby, C. W.; Goward, G. R., The Challenge of Paramagnetism in Two-Dimensional ^{6,7}Li Exchange NMR. *App. Mag. Res.* **2007,** *32*, 565-581.
3. Blank, F.; Leskes, M.; Grey, C. P., In Situ Solid-State NMR Spectroscopy of Electrochemical Cells: Batteries, Supercapacitors, and Fuel Cells. *Acc. Chem. Res.* **2013,** *46* (9), 1952-1963.
4. Spencer, T. L.; Plagos, N. W.; Brouwer, D. H.; Goward, G. R., The use of ^{6}Li{^{7}Li}-REDOR NMR Spectroscopy to Compare the Ionic Conductivities of Solid-State Lithium Ion Electrolytes. *Phys. Chem. Chem. Phys.* **2014,** *16*, 2515-2526.
5. Mizushima, K.; Jones, P. C.; Wiseman, P. J.; Goodenough, J. B., Li_XCoO_2 (0<X<-1): A New Cathode Material for Batteries of High Energy Density. *Mater. Res. Bull.* **1980,** *15* (6), 783-789.

6. Kao, H. M.; Hung, T. T.; Fey, G. T. K., Multinuclear Solid-State NMR Characterization, Ion Dissociation, and Dynamic Properties of Lithium-Doped Organic-Inorganic Hybrid Electrolytes Based on Ureasils. *Macromolecules* **2007,** *40*, 8673-8683.
7. Ogorodnikov, I. N.; Pustovarov, V. A.; Kirm, M.; Kruzhalov, A. V.; Isaenko, L. I., Electron Excitations in LiB_3O_5 Crystals with Defects: Low-Temperature Time-Resolved Luminescence Vuv Spectroscopy. *Phys. Solid State* **2001,** *43* (8), 1454-1463.
8. Massot, O.; Rousselle, J. C.; Fillion, M. P.; Januel, D.; Plantefol, M.; Fillion, G., 5-HT1B Receptors: A Novel Target for Lithium. Possible Involvement in Mood Disorders. *Neuropsychopharmacology* **1999,** *21*, 530-541.
9. Denry, I.; Holloway, J., Ceramics for Dental Applications: A Review. *Materials* **2010,** *3* (1), 351.
10. Darling, M.; Hill, R., Novel Polyalkenoate (Glass-Ionomer) Dental Cements Based on Zinc Silicate Glasses. *Biomaterials* **1994,** *15* (4), 299-306.
11. Idota, Y.; Kubota, T.; Matsufuji, A.; Maekawa, Y.; Miyasaka, T., Tin-Based Amorphous Oxide: A High-Capacity Lithium-Ion-Storage Material. *Science* **1997,** *276*, 1395-1397.
12. Stebbins, J. F.; Farnan, I., Effects of High Temperature on Silicate Liquid Structure: A Multinuclear NMR Study. *Science* **1992,** *255*, 586-589.
13. Xu, Z.; Stebbins, J. F., Cation Dynamics and Diffusion in Lithium Orthosilicate: Two-Dimensional Lithium-6 NMR. *Science* **1995,** *270* (5240), 1332-1334.
14. Xu, Z.; Stebbins, J. F., ^{6}Li Nuclear Magnetic Resonance Chemical Shifts, Coordination Number and Relaxation in Crystalline & Glassy Silicates. *Solid State Nucl. Magn. Reson.* **1995,** *5*, 103-112.
15. Bohmer, R.; Jeffrey, K. R.; Vogel, M., Solid State Li NMR with Application to the Translational Dynamics in Ion Conductors. *Prog. Nucl. Mag. Res. Spectro.* **2007,** *50*, 87-174.
16. Lee, Y. J.; Grey, C. P., Determining the Lithium Local Environments in the Lithium Manganates $LiZn_{0.5}Mn_{1.5}O_4$ and Li_2MnO_3 by Analysis of the ^{6}Li MAS NMR Spinning Sideband Manifolds. *J. Phys. Chem. B* **2002,** *106* (14), 3576-3582.
17. Tucker, M. C.; Reimer, J. A.; Cairns, E. J., ^{7}Li NMR Studies of Chemically-Delithiated $Li_{1-x}CoO_2$. *J. Phys. Chem. B* **2002,** *106* (15), 3842-3847.
18. Youngman, R., NMR Spectroscopy in Glass Science: A Review of the Elements. *Materials* **2018,** *11* (4), 476.
19. Grey, C. P.; Dupré, N., NMR Studies of Cathode Materials for Lithium-Ion Rechargeable Batteries. *Chem. Rev.* **2004,** *104* (10), 4493-4512.
20. Blanc, F.; Leskes, M.; Grey, C. P., In Situ Solid-State NMR Spectroscopy of Electrochemical Cells: Batteries, Supercapacitors, and Fuel Cells. *Acc. Chem. Res.* **2013,** *46* (9), 1952-1963.
21. Breger, J.; Meng, Y. S.; Hinuma, Y.; Kumar, S.; Kang, K.; Shao-Horn, Y.; Ceder, G.; Grey, C. P., Effect of High Voltage on the Structure and Electrochemistry of $LiNi_{0.5}Mn_{0.5}O_2$: A Joint Experiment and Theoretical Study. *Chem. Mater.* **2006,** *18*, 4768-4781.
22. Kang, K.; Meng, Y. S.; Breger, J.; Grey, C. P.; Ceder, G., Electrodes with High Power and High Capacity for Rechargeable Lithium Batteries. *Science* **2006,** *311* (5763), 977-980.
23. Mackenzie, K. J. D.; Smith, M. E., *Multinuclear Solid-State NMR of Inorganic Materials*. Pergamon: London, 2002; Vol. 6, p 727.
24. Waugh, J. S.; Huber, L. M.; Haeberle, U., Approach to High Resolution NMR in Solids. *Phys. Rev. Lett.* **1968,** *20* (5), 180.
25. Taylor, R. E.; Pembleton, R. G.; Ryan, L. M.; Gerstein, B. C., Combined Multiple Pulse NMR and Sample Spinning: Recovery of Proton Chemical Shift. *J. Chem. Phys.* **1979,** *71*, 4541-4545.
26. Lee, M.; Goldburg, W. I., Nuclear-Magnetic-Resonance Line Narrowing by a Rotating RF Field. *Phys. Rev. A* **1965,** *140*, 1261.
27. Nishiyama, Y.; Malon, M.; Gan, Z.; Endo, Y.; Nemoto, T., Proton–Nitrogen-14 Overtone Two-Dimensional Correlation NMR Spectroscopy of Solid-Sample at Very Fast Magic Angle Sample Spinning. *J. Magn. Reson.* **2013,** *230*, 160-164.
28. Agarwal, V.; Penzel, S.; Szekely, K.; Cadalbert, R.; Testori, E.; Oss, A.; Past, J.; Samoson, A.; Ernst, M.; Böckmann, A.*, et al.*, De Novo 3D Structure Determination from Sub-Milligram Protein Samples by Solid-State 100 kHz MAS NMR Spectroscopy. *Angew. Chem. Int. Ed.* **2014,** *53* (45), 12253-12256.
29. Kobayashi, T.; Mao, K.; Paluch, P.; Nowak-Król, A.; Sniechowska, J.; Nishiyama, Y.; Gryko, D. T.; Potrzebowski, M. J.; Pruski, M., Study of Intermolecular Interactions in the Corrole Matrix by Solid-State NMR under 100 kHz MAS and Theoretical Calculations. *Angew. Chem. Int. Ed.* **2013,** *52* (52), 14108-14111.
30. Ye, Y. Q.; Malon, M.; Martineau, C.; Taulelle, F.; Nishiyama, Y., Rapid Measurement of Multidimensional H-1 Solid-State NMR Spectra at Ultra-Fast MAS Frequencies. *J. Magn. Reson.* **2014,** *239*, 75-80.
31. Asami, S.; Reif, B., Proton-Detected Solid-State NMR Spectroscopy at Aliphatic Sites: Application to Crystalline Systems. *Acc. Chem. Res.* **2013,** *46* (9), 2089-2097.
32. McDermott, A. E.; Creuzet, F. J.; Kolbert, A. C.; Griffin, R. G., High-Resolution Magic-Angle-Spinning NMR Spectra of Protons in Deuterated Solids. *J. Magn. Reson. (1969)* **1992,** *98* (2), 408-413.
33. Paulson, E. K.; Morcombe, C. R.; Gaponenko, V.; Dancheck, B.; Byrd, R. A.; Zilm, K. W., Sensitive High Resolution Inverse Detection NMR Spectroscopy of Proteins in the Solid State. *J. Am. Chem. Soc.* **2003,** *125* (51), 15831-15836.
34. Reif, B.; Jaroniec, C. P.; Rienstra, C. M.; Hohwy, M.; Griffin, R. G., ^{1}H–^{1}H MAS Correlation Spectroscopy and Distance Measurements in a Deuterated Peptide. *J. Magn. Reson.* **2001,** *151* (2), 320-327.
35. Zhou, D. H.; Graesser, D. T.; Franks, W. T.; Rienstra, C. M., Sensitivity and Resolution in Proton Solid-State NMR at Intermediate Deuteration Levels: Quantitative Linewidth Characterization and Applications to Correlation Spectroscopy. *J. Magn. Reson.* **2006,** *178* (2), 297-307.
36. McDermott, A. E.; Creuzet, F. J.; Kolbert, A. C.; Griffin, R. G., High-Resolution Magic-Angle-Spinning NMR Spectra of Protons in Deuterated Solids. *J. Magn. Reson.* **1992,** *98*, 408-413.
37. Zheng, L.; Fishbein, K. W.; Griffin, R. G.; Herzfeld, J., Two-Dimensional Solid-State ^{1}H NMR and Proton Exchange. *J. Am. Chem. Soc.* **1993,** *115*, 6254-6261.
38. Barbet-Massin, E.; Pell, A. J.; Retel, J. S.; Andreas, L. B.; Jaudzems, K.; Franks, W. T.; Nieuwkoop, A. J.; Hiller, M.; Higman, V.; Guerry, P.*, et al.*, Rapid Proton-Detected NMR Assignment for Proteins with Fast Magic Angle Spinning. *J. Am. Chem. Soc.* **2014,** *136* (35), 12489-12497.
39. Chevelkov, V.; Rehbein, K.; Diehl, A.; Reif, B., Ultrahigh Resolution in Proton Solid-State NMR Spectroscopy at High Levels of Deuteration. *Angew. Chem. Int. Ed.* **2006,** *45* (23), 3878-3881.
40. Lewandowski, J. Z. R.; Dumez, J.-N.; Akbey, U. m.; Lange, S.; Emsley, L.; Oschkinat, H., Enhanced Resolution and Coherence Lifetimes in the Solid-State NMR Spectroscopy of Perdeuterated Proteins under Ultrafast Magic-Angle Spinning. *J. Phys. Chem. Lett.* **2011,** *2* (17), 2205-2211.
41. Bengisu, M., Borate Glasses for Scientific and Industrial Applications: A Review. *J. Mater. Sci.* **2016,** *51* (5), 2199-2242.
42. Lelong, G.; Cormier, L.; Hennet, L.; Michel, F.; Rueff, J.-P.; Ablett, J. M.; Monaco, G., Lithium Borate Crystals and Glasses: How Similar Are They? A Non-Resonant Inelastic X-Ray Scattering Study around the B and O K-Edges. *J. Non-Cryst. Solids* **2017,** *472*, 1-8.
43. Stewner, V. F., Die Kristallstruktur Von α-Li_3BO_3. *Acta Cryst.* **1971,** *B27*, 904-910.
44. Lelong, G.; Radtke, G.; Cormier, L.; Bricha, H.; Rueff, J.-P.; Ablett, J. M.; Cabaret, D.; Gélébart, F.; Shukla, A., Detecting Non-Bridging Oxygens: Non-Resonant Inelastic X-Ray Scattering in Crystalline Lithium Borates. *Inorg. Chem.* **2014,** *53* (20), 10903-10908.
45. Rousse, G.; Baptiste, B.; Lelong, G., Crystal Structures of $Li_6B_4O_9$ and $Li_3B_{11}O_{18}$ and Application of the Dimensional Reduction Formalism to Lithium Borates. *Inorg. Chem.* **2014,** *53* (12), 6034-6041.
46. Cahill, L. S.; Yin, S. C.; Samoson, A.; Heinmaa, I.; Nazar, L. F.; Goward, G. R., ^{6}Li NMR Studies of Cation Disorder and Transition Metal Ordering in $Li[Ni_{1/3}Mn_{1/3}Co_{1/3}]O_2$ Using Ultrafast Magic Angle Spinning. *Chem. Mater.* **2005,** *17* (26), 6560-6566.
47. Pan, C.; Lee, Y. J.; Ammundsen, B.; Grey, C. P., ^{6}Li MAS NMR Studies of the Local Structure and Electrochemical Properties of Cr-Doped Lithium Manganese and Lithium Cobalt Oxide Cathode Materials for Lithium-Ion Batteries. *Chem. Mater.* **2002,** *14* (5), 2289-2299.
48. Messinger, R. J.; Ménétrier, M.; Salager, E.; Boulineau, A.; Duttine, M.; Carlier, D.; Ateba Mba, J.-M.; Croguennec, L.; Masquelier, C.; Massiot, D.*, et al.*, Revealing Defects in Crystalline Lithium-Ion Battery Electrodes by Solid-State NMR: Applications to $LiVPO_4F$. *Chem. Mater.* **2015,** *27* (15), 5212-5221.
49. Vinod Chandran, C.; Heitjans, P., Chapter One - Solid-State NMR Studies of Lithium Ion Dynamics across Materials Classes. In *Annu. Rep. NMR Spectrosc.*, Webb, G. A., Ed. Academic Press: 2016; Vol. 89, pp 1-102.

50. Michaelis, V. K.; Aguiar, P. M.; Kroeker, S., Probing Alkali Coordination Environments in Alkali Borate Glasses by Multinuclear Magnetic Resonance. *J. Non-Cryst. Solids* **2007,** *353* (26), 2582-2590.
51. Kroeker, S.; Stebbins, J. F., Three-Coordinated Boron-11 Chemical Shifts in Borates. *Inorg. Chem.* **2001,** *40*, 6239-6246.
52. Engelhardt, G.; Michel, D., *High-Resolution Solid-State NMR of Silicates and Zeolites*. John Wiley & Sons: 1987; p 485.
53. George, A. M.; Sen, S.; Stebbins, J. F., ^{23}Na Chemical Shifts and Local Structure in Crystalline, Glassy, and Molten Sodium Borates and Germanates. *Solid State Nucl. Magn. Reson.* **1997,** *10*, 9-17.
54. Fiske, P. S.; Stebbins, J. F., The Structual Role of Mg in Silicate Liquids: A High-Temperature ^{25}Mg, ^{23}Na and ^{29}Si NMR Study. *Amer. Min.* **1994,** *79*, 848-861.
55. Kroeker, S.; Stebbins, J. F., Magnesium Coordination Environments in Glasses and Minerals: New Insight from High-Field Magnesium-25 MAS NMR. *Amer. Min.* **2000,** *85*, 1459-1464.
56. Cherry, B. R.; Nyman, M.; Alam, T. M., Investigation of Cation Environment and Framework Changes in Silicotitanate Exchange Materials Using Solid-State ^{23}Na, ^{29}Si, and ^{133}Cs MAS NMR. *J. Solid State Chem.* **2004,** *177*, 2079-2093.
57. Michaelis, V. K.; Kroeker, S., ^{73}Ge Solid-State NMR of Germanium Oxide Materials: Experimental and Theoretical Studies. *J. Phys. Chem. C* **2010,** *114* (49), 21736-21744.
58. Zhou, B.; Faucher, A.; Laskowski, R.; Terskikh, V. V.; Kroeker, S.; Sun, W.; Lin, J.; Mi, J.-X.; Michaelis, V. K.; Pan, Y., Ultrahigh-Field ^{25}Mg NMR and DFT Study of Magnesium Borate Minerals. *ACS Earth Space Chem.* **2017,** *1* (6), 299-309.
59. Addison, A. W.; Rao, T. N.; Reedijk, J.; van Rijn, J.; Verschoor, G. C., Synthesis, Structure, and Spectroscopic Properties of Copper(II) Compounds Containing Nitrogen-Sulphur Donor Ligands; the Crystal and Molecular Structure of Aqua[1,7-Bis(N-Methylbenzimidazol-2[Prime or Minute]-Yl)-2,6-Dithiaheptane]Copper(II) Perchlorate. *J. Chem. Soc., Dalt. Trans.* **1984,** (7), 1349-1356.
60. Vijayakumar, M.; Kerisit, S.; Yang, Z.; Graff, G. L.; Liu, J.; Sears, J. A.; Burton, S. D.; Rosso, K. M.; Hu, J., Combined ^{6,7}Li NMR and Molecular Dynamics Study of Li Diffusion in Li_2TiO_3. *J. Phys. Chem. C* **2009,** *113* (46), 20108-20116.
61. Wiedemann, D.; Nakhal, S.; Rahn, J.; Witt, E.; Islam, M. M.; Zander, S.; Heitjans, P.; Schmidt, H.; Bredow, T.; Wilkening, M.*, et al.*, Unravelling Ultraslow Lithium-Ion Diffusion in ɣ-$LiAlO_2$: Experiments with Tracers, Neutrons, and Charge Carriers. *Chem. Mater.* **2016,** *28* (3), 915-924.
62. Fu, K.; Gong, Y.; Liu, B.; Zhu, Y.; Xu, S.; Yao, Y.; Luo, W.; Wang, C.; Lacey, S. D.; Dai, J.*, et al.*, Toward Garnet Electrolyte–Based Li Metal Batteries: An Ultrathin, Highly Effective, Artificial Solid-State Electrolyte/Metallic Li Interface. *Sci. Adv.* **2017,** *3* (4), e1601659.
63. Han, X.; Gong, Y.; Fu, K.; He, X.; Hitz, G. T.; Dai, J.; Pearse, A.; Liu, B.; Wang, H.; Rubloff, G.*, et al.*, Negating Interfacial Impedance in Garnet-Based Solid-State Li Metal Batteries. *Nature Mater.* **2016,** *16*, 572-579.
64. Concistrè, M.; Johannessen, O. G.; Carignani, E.; Geppi, M.; Levitt, M. H., Magic-Angle Spinning NMR of Cold Samples. *Acc. Chem. Res.* **2013,** *46* (9), 1914-1922.
65. Tycko, R., NMR at Low and Ultralow Temperatures. *Acc. Chem. Res.* **2013,** *46* (9), 1923-1932.
66. Bouleau, E.; Saint-Bonnet, P.; Mentink-Vigier, F.; Takahashi, H.; Jacquot, J. F.; Bardet, M.; Aussenac, F.; Purea, A.; Engelke, F.; Hediger, S.*, et al.*, Pushing NMR Sensitivity Limits Using Dynamic Nuclear Polarization with Closed-Loop Cryogenic Helium Sample Spinning. *Chem. Sci.* **2015,** *6* (12), 6806-6812.
67. Ha, M.; Michaelis, V. K., High-Frequency Dynamic Nuclear Polarization NMR for Solids: Part 1 – an Introduction. In *Modern Magnetic Resonance*, Webb, G. A., Ed. Springer International Publishing: Cham, 2017.
68. Chaudhari, S. R.; Berruyer, P.; Gajan, D.; Reiter, C.; Engelke, F.; Silverio, D. L.; Coperet, C.; Lelli, M.; Lesage, A.; Emsley, L., Dynamic Nuclear Polarization at 40 kHz Magic Angle Spinning. *Phys. Chem. Chem. Phys.* **2016,** *18* (15), 10616-10622.

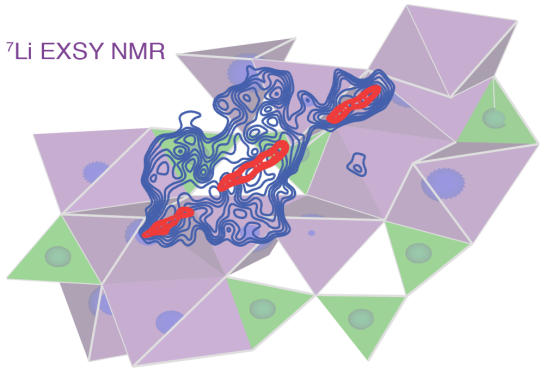
^{7}Li EXSY NMR